Supplementary Material for "Volcano transition in a solvable model of frustrated oscillators"

Bertrand Ottino-Löffler and Steven H. Strogatz
Center for Applied Mathematics, Cornell University, Ithaca, New York 14853
(Dated: May 18, 2018)

Appendix A: Independence of entries of $J_{j,k}$.

Proposition: Nontrivial pairs of entries of

$$J_{jk} = \frac{J}{N}\sum_{m=1}^{K}(-1)^m u_m^{(j)} u_m^{(k)},$$

are independent, given all the $u_m^{(j)}$ are ± 1 with equal probability.

Proof: We are going to ignore comparing J_{jk} with J_{kj}, since the enforced symmetry makes these always equal, and thus trivially dependent. We will also avoid comparing any entry with J_{jj}, since the entire diagonal is always 0, so independence is trivial.

Comparing J_{jk} with J_{lp} is likewise trivial, given j, k, l, p all distinct – they represent independent sums of independent random variables, so independence is assured.

The only case which is potentially nontrivial is comparing J_{jk} with J_{jl}, given j, k, l all distinct. The cases of J_{jl} vs. J_{kj}, J_{lj} vs. J_{jk}, and J_{lj} vs. J_{kj} are redundant, due to matrix symmetry.

To show independence of J_{jk} with J_{jl}, we directly compute the joint probability, which is

$$\begin{aligned}\mathcal{P} &:= P\left(\frac{N}{J}J_{jk} = 2x - K \text{ and } \frac{N}{J}J_{jl} = 2y - K\right)\\ &= P\left(\sum_{m=1}^{K}(-1)^m u_m^{(j)}u_m^{(k)} = 2x - K \text{ and } \sum_{m=1}^{K}(-1)^m u_m^{(j)}u_m^{(l)} = 2y - K\right).\end{aligned}$$

To simplify our terminology, we define $a_m := (-1)^m u_m^{(j)}$, $b_m := u_m^{(k)}$, $c_m := u_m^{(l)}$. Each of a, b, and c are independent sequences of independent random variables, each with equal probability of being ± 1. Therefore, each can be thought of as a fair K-long coinflip sequence of $+1$'s and -1's.

$$\begin{aligned}\mathcal{P} &= P\left(\sum_{m=1}^{K} a_m b_m = 2x - K \text{ and } \sum_{m=1}^{K} a_m c_m = 2y - K\right)\\ &= P\,(\text{ coinflip sequence } a \text{ agrees with } b \ x \text{ times and with } c \ y \text{ times })\end{aligned}$$

From here, it is obvious that because a, b, and c are independent, the joint probability becomes

$$\begin{aligned}\mathcal{P} &= \binom{K}{x}\binom{K}{y}2^{-2K}\\ &= P\left(\frac{N}{J}J_{jk} = 2x - K\right)P\left(\frac{N}{J}J_{jl} = 2y - K\right).\end{aligned}$$

Therefore, independence is assured.

Appendix B: Using the Ott-Antonsen ansatz (I)

Here, we will expand on manipulations that start with the Ott-Antonsen ansatz,

$$f(\theta, \omega, u, t) = \frac{1}{2\pi}\left[1 + \sum_{n=1}^{\infty}\alpha(\omega, u, t)^n e^{in\theta} + \text{c.c.}\right],$$

and the dynamics

$$\nu(\theta,\omega,u,t)=\omega+\frac{1}{2i}\left[e^{-i\theta}P(u,t)-e^{i\theta}P^*(u,t)\right],$$

and end with the ODE

$$\dot{a}(u,t)=-a(u,t)+\frac{P^*(u,t)-a(u,t)^2P(u,t)}{2}.$$

Because we are working in a continuum limit, our main step will be applying the following continuity equation:

$$-f_t=(f\nu)_\theta.$$

First, we evaluate the left-hand side by inserting the Ott-Antonsen ansatz, namely

$$\begin{aligned}-f_t=&\partial_t\frac{-1}{2\pi}\left[1+\sum_{n=1}^{\infty}\alpha(\omega,u,t)^ne^{in\theta}+\text{c.c.}\right]\\=&\frac{-1}{2\pi}\sum_{n=1}^{\infty}\left(n\dot{\alpha}\alpha^{n-1}e^{in\theta}+n\dot{\alpha}^*\alpha^{*n-1}e^{-in\theta}\right)\end{aligned}$$

To evaluate the right-hand side, we first product our ansatz with the dynamics to get

$$\begin{aligned}f\nu=&\frac{1}{2\pi}\left[1+\sum_{n=1}^{\infty}\alpha^ne^{in\theta}+\alpha^*ne^{-in\theta}\right]\left[\omega+\frac{1}{2i}\left(e^{-i\theta}P-e^{i\theta}P^*\right)\right]\\=&\frac{1}{4\pi i}\left[2\omega i+\alpha P-\alpha^*P^*\right]\\&+\frac{1}{4\pi i}\sum_{n=1}^{\infty}\left(2\omega i\alpha^n+\alpha^{n+1}P-\alpha^{n-1}P^*\right)e^{in\theta}\\&+\frac{1}{4\pi i}\sum_{n=1}^{\infty}\left(2\omega i\alpha^{*n}-\alpha^{*n+1}P^*+\alpha^{*n-1}P\right)e^{-in\theta}.\end{aligned}$$

Meaning that the right-hand side evaluates to

$$\begin{aligned}(f\nu)_\theta=&\frac{1}{4\pi i}\sum_{n=1}^{\infty}(in)\left(2\omega i\alpha^n+\alpha^{n+1}P-\alpha^{n-1}P^*\right)e^{in\theta}\\&+\frac{1}{4\pi i}\sum_{n=1}^{\infty}(-in)\left(2\omega i\alpha^{*n}-\alpha^{*n+1}P^*+\alpha^{*n-1}P\right)e^{-in\theta}.\end{aligned}$$

From here, it is just a matter of seeing $f_t+(f\nu)_\theta=0$ and setting Fourier coefficients to be equal. So

$$\dot{\alpha}=-\omega\alpha i+\frac{P^*-\alpha^2P}{2}.$$

To obtain the exact ODE from the start of this section, we use a result from the next section. In particular, the calculation of $P(u,t)$ reveals it only depends on $\alpha(-i,u,t)$. So by setting $\omega=-i$ and $a(u,t):=\alpha(-i,u,t)$, we finally get

$$\dot{a}(u,t)=-a(u,t)+\frac{P^*(u,t)-a(u,t)^2P(u,t)}{2}.$$

Appendix C: Using the Ott-Antonsen ansatz (II)

Here, we will elaborate on how the local field

$$P(u,t) = \langle J(u,u')e^{i\theta'} \rangle$$

becomes

$$P(u,t) = \frac{J}{2^K} \sum_{u'} \sum_{m=1}^{K} (-1)^m u_m u'_m a^*(u',t)$$

under the Ott-Antonsen ansatz.

The first step is to insert the Ott-Antonsen ansatz into the integral to get

$$\begin{aligned} P(u,t) &= \int J(u,u')e^{i\theta'} f(\theta',\omega',u',t) g(\omega')\rho(u') d\theta' d\omega' du' \\ &= \int \frac{J(u,u')}{2\pi} \left[e^{i\theta'} + \sum_{n=1}^{\infty} \alpha^n e^{i(n+1)\theta} + \alpha^* n e^{-i(n-1)\theta} \right] g(\omega')\rho(u') d\theta' d\omega' du'. \end{aligned}$$

By taking the integral over θ, everything but the $n = 1$ term of the sum evaluates to 0. So

$$P(u,t) = \int J(u,u')\alpha^* g(\omega')\rho(u') d\omega' du'.$$

Next, we want to take the ω' integral. Since we are using a Cauchy distribution, then

$$g(\omega) = \frac{1}{\pi(a+\omega^2)} = \frac{i/(2\pi)}{\omega + i} + \frac{-i/(2\pi)}{\omega - i}.$$

So if α has the appropriate smoothness and decay (see ref [1] for more details), then the integrand has exactly two poles, one at each of $\pm i$. So, by taking the appropriate contour integral (i.e., one which runs around across the real line and semicircles around in the bottom half-plane), we get

$$\begin{aligned} P(u,t) &= \int J(u,u') \left(\int \alpha^*(\omega',u',t) g(\omega') d\omega' \right) \rho(u') du' \\ &= \int J(u,u') \left(-2\pi i \frac{i}{2\pi} \alpha^*(-i,u',t) \right) \rho(u') du' \\ &= \int J(u,u') a(u',t) \rho(u') du', \end{aligned}$$

where $a(u,t) := \alpha(-i,u,t)$. Incidentally, this is why the last section involves an evaluation of $\omega = -i$.

From here, all we need to do is just plug in for $J(u,u')$, recalling that $\rho(u') = 2^{-K} \sum_v \delta(u'-v)$. Therefore,

$$\begin{aligned} P(u,t) &= \int J(u,u') a(u',t) \rho(u') du' \\ &= \frac{J}{2^K} \sum_{u'} \sum_{m=1}^{K} (-1)^m u_m u'_m a^*(u',t), \end{aligned}$$

completing the section.

Appendix D: $\zeta_v^{(n)}$ as eigenvectors

Proposition: Given K even and using indices $u, v \in \{\pm 1\}^K$, then for any $n \in \{1, \ldots, K\}$, then

$$\zeta_v^{(n)} = v_n$$

is an eigenvector of

$$A_{uv} = \sum_{m=1}^{K} (-1)^m u_m v_m.$$

Proof: This will be attacked directly. Let us fix some $n \in \{1, 2, \ldots, K\}$ and $u \in \{+1, -1\}^K$. So

$$\begin{aligned}
\left(A\zeta^{(n)}\right)_u &= \sum_v A_{uv}\zeta_v^{(n)} = \sum_v \left(\sum_{m=1}^{K} (-1)^m u_m v_m\right) v_n \\
&= \sum_{m=1}^{K} \sum_v (-1)^m u_m v_m v_n \\
&= \sum_v (-1)^n u_n v_n v_n + \sum_{m \neq n} \sum_v (-1)^m u_m v_m v_n \\
&= \text{Term 1} + \text{Term 2},
\end{aligned}$$

where each "Term" will be simplified on its own.

The first term reduces rather quickly, as in

$$\begin{aligned}
\text{Term 1} &= \sum_v (-1)^n u_n v_n v_n \\
&= (-1)^n u_n \sum_v v_n^2 \\
&= (-1)^n 2^K u_n.
\end{aligned}$$

The second term is somewhat more complicated, where we reduce it into

$$\begin{aligned}
\text{Term 2} &= \sum_{m \neq n} \sum_{v \in \{\pm 1\}^K} (-1)^m u_m v_m v_n \\
&= \sum_m \sum_{v' \in \{\pm 1\}^{K-1}} u'_m v'_m,
\end{aligned}$$

where the u' and v' are n-deleted versions of $(-1)^m u_m$ and $v_m v_n$ specifically. However, this means that evaluating this term becomes a matter of just counting the number of places two vectors u' and v' of length $K-1$ disagree, across all possible v'. So, combinatorically, it becomes

$$\text{Term 2} = 2 \sum_{w=0}^{K-1} (K - 1 - 2w) \binom{K-1}{w}.$$

However, this becomes the sum across an odd function across $K/2$ (using the evenness of K), so this term immediately evaluates to 0.

Therefore,

$$\begin{aligned}
\left(A\zeta^{(n)}\right)_u &= \text{Term 1} + \text{Term 2} \\
&= (-1)^n 2^K u_n + 0 \\
&= (-1)^n 2^K u_n.
\end{aligned}$$

This holds for all u, so for all n we have

$$A\zeta^{(n)} = (-1)^n 2^K \zeta^{(n)}.$$

Appendix E: Demonstration of nullspace of A

Proposition: Using the same setup as the previous section,

$$\eta \perp \zeta^{(n)} \text{ for all } n$$

implies

$$A\eta = 0.$$

Proof: Let us choose some η orthogonal to all $\zeta^{(n)}$. Then for any $n = 1, 2, \ldots, K$, we have

$$\eta\zeta^{(n)} = 0.$$

Therefore, by direct computation,

$$\begin{aligned}(A\eta)_u &= \sum_v A_{uv}\eta_u = \sum_v \sum_{m=1}^{K} (-1)^m u_m v_m \eta_u \\ &= \sum_{m=1}^{K} (-1)^m u_m \sum_v v_m \eta_u = \sum_{m=1}^{K} (-1)^m u_m \left(\eta\zeta^{(n)}\right) \\ &= \sum_{m=1}^{K} (-1)^m u_m 0 = 0.\end{aligned}$$

So $A\eta = 0$.

Appendix F: Demonstration of concavity

Proposition: The sum of symmetric normals centered at $\pm\mu$ with individual variances σ^2, that is,

$$h(r) = \frac{2}{\sqrt{2\pi\sigma^2}} \exp\left(\frac{-\mu^2 - r^2}{2\sigma^2}\right) \cosh\left(\frac{\mu r}{\sigma^2}\right),$$

is concave down at the origin whenever $\mu^2/\sigma^2 < 1$ and concave up at the origin whenever $\mu^2/\sigma^2 > 1$.

Proof: Letting $\gamma := \mu^2/\sigma^2$ and $\beta := \mu/\sigma^2$, the distribution becomes

$$h(r) = \frac{2\beta}{\sqrt{2\pi\gamma}} \exp\left(\frac{-\gamma}{2}\right) \exp\left(\frac{-r^2\beta^2}{2\gamma}\right) \cosh(r\beta).$$

From here direct computation reveals

$$\partial_r^2 h(r) = \beta^3\gamma^{-2} \exp\left(\frac{-\gamma}{2} - \frac{\beta^2 r^2}{2\gamma}\right) \sqrt{\frac{2}{\pi\gamma}} \cosh(\beta r) \left[-\gamma + \gamma^2 + \beta^2 r^2 - 2\beta\gamma r \tanh(\beta r)\right].$$

Evaluating therefore gives

$$\partial_r^2 h(0) = \beta^3\gamma^{-1} \exp(-\gamma/2) \sqrt{\frac{2}{\pi\gamma}} (\gamma - 1).$$

So h is concave down whenever $\gamma < 1$ and concave up whenever $\gamma > 1$.

Appendix G: Derivation of $M_{+1}M_{-1}$

Proposition: The product of the first and negative first moments of the fitted 2D radial distribution is

$$M_{+1}M_{-1} = \frac{\pi}{2}\frac{1+\gamma}{[e^{-\gamma/2} + \sqrt{\pi\gamma/2}\text{Erf}(\sqrt{\gamma/2})]^2}$$

where $\gamma = \mu^2/\sigma^2$.

Proof: The distribution in question we plan on using is

$$h(r) = \frac{2}{\sqrt{2\pi\sigma^2}} \exp\left(\frac{-\mu^2 - r^2}{2\sigma^2}\right) \cosh\left(\frac{\mu r}{\sigma^2}\right),$$

for $r \geq 0$. We start by defining

$$\mu_n := \int_0^\infty r^n h(r) dr.$$

By direct computation, and by setting $\beta = \mu/\sigma^2$, we get

$$\begin{aligned}
\mu_0 &= 1, \\
\mu_1 &= e^{-\gamma/2}\sqrt{\frac{2\gamma}{\pi}}\frac{1}{\beta} + \frac{\gamma}{\beta}\text{Erf}\left(\sqrt{\frac{\gamma}{2}}\right), \\
\mu_2 &= \frac{\gamma^2 + \gamma}{\beta^2}.
\end{aligned}$$

However, notice that $h(r)$ is just a 1D density on $(0, \infty)$. To get the 2D distribution which we will be sampling from, we need to rotate it and renormalize. So the "true" distribution we are sampling is closer to

$$H(x, y) := \frac{h\left(\sqrt{x^2 + y^2}\right)}{2\pi\mu_1},$$

since it has the correct radial behavior, is rotationally symmetric, and is properly normalized on the plane. So the moments we are numerically observing are simply

$$\begin{aligned}
M_n &= \int\int H(x, y)\left(\sqrt{x^2 + y^2}\right)^n dxdy \\
&= \int\int r^n \frac{h(r)}{2\pi\mu_1} r dr d\theta \\
&= \frac{\mu_{n+1}}{\mu_1}.
\end{aligned}$$

By plugging in our earlier computations, we therefore get the first and negative first moments to be

$$\begin{aligned}
M_{-1} &= \frac{\mu_0}{\mu_1} = \frac{\beta}{e^{-\gamma/2}\sqrt{\frac{2\gamma}{\pi}} + \gamma\text{Erf}\left(\sqrt{\frac{\gamma}{2}}\right)} \\
M_{+1} &= \frac{\mu_2}{\mu_1} = \frac{(\gamma^2 + \gamma)/\beta}{e^{-\gamma/2}\sqrt{\frac{2\gamma}{\pi}} + \gamma\text{Erf}\left(\sqrt{\frac{\gamma}{2}}\right)}.
\end{aligned}$$

All the β dependency cancels out, so we get the desired expression:

$$M_{+1}M_{-1} = \frac{\pi}{2}\frac{1+\gamma}{[e^{-\gamma/2} + \sqrt{\pi\gamma/2}\text{Erf}(\sqrt{\gamma/2})]^2}.$$

Appendix H: Numerically estimating $M_{+1}M_{-1}$

Because it was left somewhat ambiguous in the main body, we will take a second to clarify how the product of the first and negative first moments $M_{+1}M_{-1}$ is numerically estimated.

Given the time-history of a single simulation run, we estimate individual moments from numerically obtained values of

$$P_j(t) = x_j(t) + iy_j(t) := \sum_{k=1}^{N} J_{jk} \left(\cos(\theta_k(t)) + i\sin(\theta_k(t))\right),$$

by averaging over all N fields and over the sampling window T. So

$$M_{+1} \approx \frac{1}{NT} \sum_{j=1}^{N} \sum_{t=1}^{T} \sqrt{x_j(t)^2 + y_j(t)^2}$$
$$M_{-1} \approx \frac{1}{NT} \sum_{j=1}^{N} \sum_{t=1}^{T} \sqrt{x_j(t)^2 + y_j(t)^2}^{-1}$$

in particular. We then run L independent simulations, with randomized initial phases, natural frequencies, and coupling matrices. We obtain averaged values of the desired moments by

$$E[M_{+1}] = \mu_{+1} \approx \frac{1}{L} \sum_{l=1}^{L} M_{+1}^{(l)}$$
$$E[M_{-1}] = \mu_{-1} \approx \frac{1}{L} \sum_{l=1}^{L} M_{-1}^{(l)}.$$

However, notice

$$E[M_{+1}M_{-1}] \neq \mu_{+1}\mu_{-1}.$$

This is because the first and negative first moments are not independent, so we run a separate average to get the moment product, so

$$E[M_{+1}M_{-1}] \approx \frac{1}{L} \sum_{l=1}^{L} M_{+1}^{(l)} M_{+1}^{(l)}.$$

To establish error, we will also need to calculate the error on this average moment product. Via standard real-time methods, we can calculate $\mathrm{Var}\left(M_{\pm 1}\right) = \sigma_{\pm 1}^2$. Properly calculating the variance on $M_{+1}M_{-1}$, is a bit more algebraically involved, but it can be shown that

$$\mathrm{Var}\left(M_{+1}M_{-1}\right) \approx \frac{1}{L}\left[\mu_{+1}^2\sigma_{-1}^2 + \mu_{-1}^2\sigma_{+1}^2 + 2\mu_{+1}\mu_{-1}\mathrm{Cov}\left(M_{+1}, M_{-1}\right)\right] + O\left(\frac{1}{L^2}\right).$$

The covariance term also be calculated via standard methods, and the L^{-2} term can be neglected given a sufficient number of replications. This establishes all the numerical tools needed to estimate $M_{+1}M_{-1}$ in any specific parameter combination.

Appendix I: Is $M_{+1}M_{-1}$ monotone in γ?

Proposition:

$$M_{+1}M_{-1} = \frac{\pi}{2} \frac{1+\gamma}{[e^{-\gamma/2} + \sqrt{\pi\gamma/2}\mathrm{Erf}(\sqrt{\gamma/2})]^2}$$

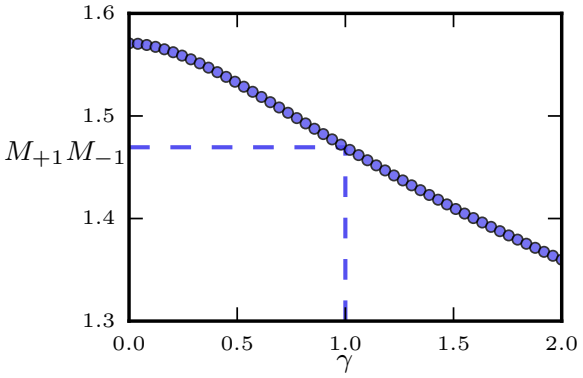

FIG. 1: Plot of $M_{+1}M_{-1}$ versus γ. Dashed lines denote $\gamma = 1$ and $M_{+1}M_{-1} \approx 1.4694$.

is monotone on $\gamma \geq 0$, allowing us to use bisection on numerically obtained moments to estimate J_C.

Proof: To make things simpler, we define a function $f(\gamma)$ where

$$\frac{\pi}{2f(\gamma)^2} = \frac{\pi}{2}\frac{1+\gamma}{[e^{-\gamma/2} + \sqrt{\pi\gamma/2}\text{Erf}(\sqrt{\gamma/2})]^2} = M_{+1}M_{-1}.$$

This is allowed since $M_{+1}M_{-1} \geq 0$ always. Notice that $M_{+1}M_{-1}$ is monotone on $\gamma \geq 0$ if and only if f is monotone. So we want to show

$$f(\gamma) = \frac{e^{-\gamma/2} + \sqrt{\pi\gamma/2}\text{Erf}(\sqrt{\gamma/2})}{\sqrt{1+\gamma}}$$

is monotone on $\gamma \geq 0$. This is equivalent to asking if

$$f'(\gamma) = \frac{\sqrt{\pi/(8\gamma)}}{(1+\gamma)^{3/2}}\left(\text{Erf}\left(\sqrt{\frac{\gamma}{2}}\right) - \sqrt{\frac{2\gamma}{\pi}}e^{-\gamma/2}\right)$$

single signed. However, recall

$$\text{Erf}\left(\sqrt{\frac{\gamma}{2}}\right) = \int_0^{\sqrt{\gamma/2}} \frac{2}{\sqrt{\pi}}e^{-t^2}dt,$$

and

$$\sqrt{\frac{\gamma}{2}}e^{-\gamma/2} = \int_0^{\sqrt{\gamma/2}} e^{-t^2} - 2t^2e^{-t^2}dt.$$

Therefore,

$$\begin{aligned} f'(\gamma) =& \frac{\sqrt{\pi/(8\gamma)}}{(1+\gamma)^{3/2}}\left(\int_0^{\sqrt{\gamma/2}} \frac{2}{\sqrt{\pi}}e^{-t^2}dt - \frac{2}{\sqrt{\pi}}\int_0^{\sqrt{\gamma/2}} e^{-t^2} - 2t^2e^{-t^2}dt\right) \\ =& \frac{\sqrt{\pi/(8\gamma)}}{(1+\gamma)^{3/2}}\int_0^{\sqrt{\gamma/2}} \frac{4}{\sqrt{\pi}}t^2e^{-t^2}dt \\ \geq& 0. \end{aligned}$$

Therefore $M_{+1}M_{-1}$ is monotone in γ. A plot of this function is provided in figure 1.

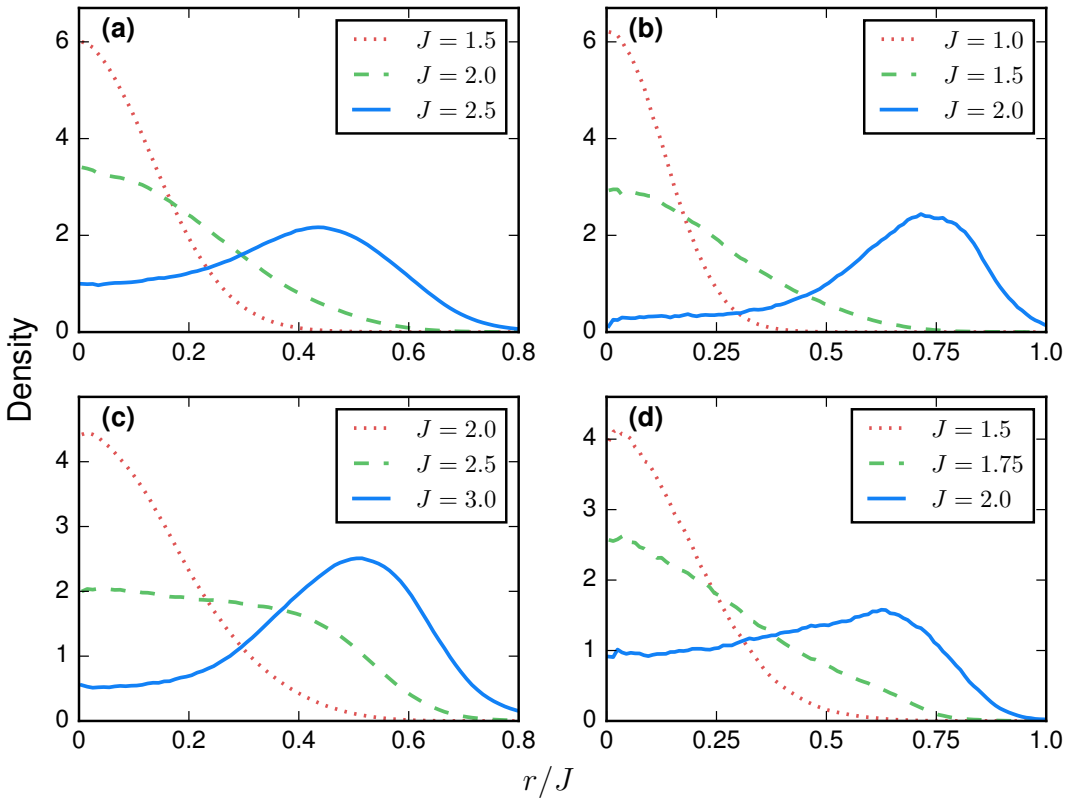

FIG. 2: Radial distribution of local fields. Each curve represents the averaged density over 500 simulations of Eq. (J1), using $N = 250$, $K = 4$, fourth-order Runge-Kutta integration with a step size of 0.01, 2000 transient steps, 4000 recorded steps, and uniformly random initial phases. (a) Coupling given by $f(x) = \sin(x)$ and natural frequencies are distributed according to a standard Cauchy. (b) Coupling given by $f(x) = \sin(x)$ and natural frequencies are distributed according to a standard normal. (c) Coupling given by $f(x) = 0.9\sin(x) + 0.1\cos(x)$ and natural frequencies are distributed according to a standard Cauchy. (d) Coupling given by $f(x) = 0.9\sin(x) + 0.1\cos(x)$ and natural frequencies are distributed according to a standard normal.

Appendix J: Generality of volcano transitions

To see if our model robustly supports volcano transitions, we use

$$\dot{\theta}_j = \omega_j + \sum_{k=1}^{N} J_{jk} f\left(\theta_k - \theta_j\right) \tag{J1}$$

as a generalization, where f is some 2π-periodic coupling function, the natural frequencies ω_j are distributed according to a density g, and the entries of J_{jk} are defined as in the main paper. Figure 2 demonstrates the existence of a volcano transition for various choices of f and g. Figure 2a recreates the setup in the main paper, with sine coupling and standard Cauchy natural frequencies. Figure 2b demonstrates the case with sine coupling and standard normal natural frequencies. Figure 2c recreates the setup in the main paper, with coupling given by $f(x) = 0.9\sin(x) + 0.1\cos(x)$ and standard Cauchy natural frequencies. Figure 2d recreates the setup in the main paper, with coupling given by $f(x) = 0.9\sin(x) + 0.1\cos(x)$ and standard normal natural frequencies. Notice how in all these cases, the density at the origin goes from concave down to concave up as J passes some critical value.

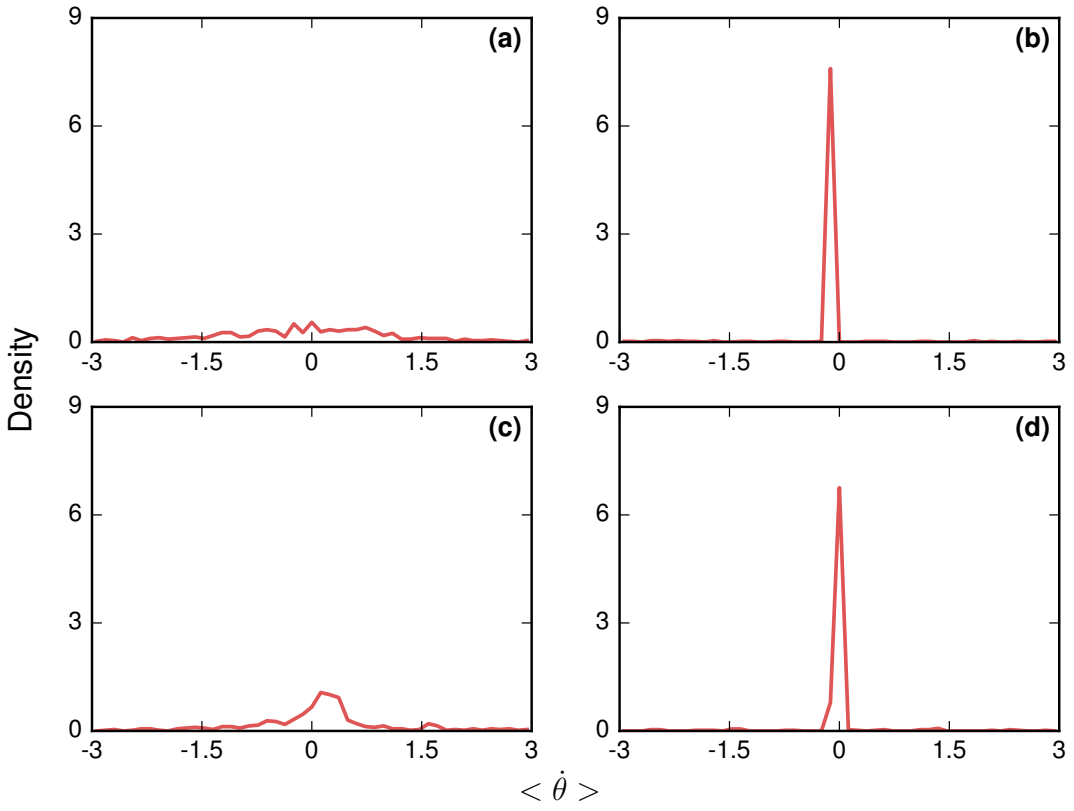

FIG. 3: Distribution of average frequencies. Each curve represents a sampled density of average frequencies of the system presented in the main text, using $N = 500$, fourth-order Runge-Kutta integration with a step size of 0.01, 5000 transient steps, 1000 recorded steps, and uniformly random initial phases. (a) $K = 2$ and $J = 1$. (b) $K = 2$ and $J = 4$. (c) $K = 500$ and $J = 1$. (d) $K = 500$ and $J = 4$.

Appendix K: Existence of locked population

One common requirement for oscillator glasses is to demand the existence of a substantial locked population of oscillators. To measure this, we numerically compute the density of average frequencies $< \dot{\theta}_j >$, and plot the results in figure 3. Figure 3a shows the distribution at low K, below the volcano transition, and displays no substantial locking. Figure 3b shows the distribution at low K, above the volcano transition, and exhibits a substantial locked population. Figure 3c shows the distribution at high K, below the volcano transition, and displays no substantial locking. Figure 3d shows the distribution at high K, above the volcano transition, and exhibits a substantial locked population. This is consistent with the observation that high K (relative to N) may correspond to the onset of a glass.

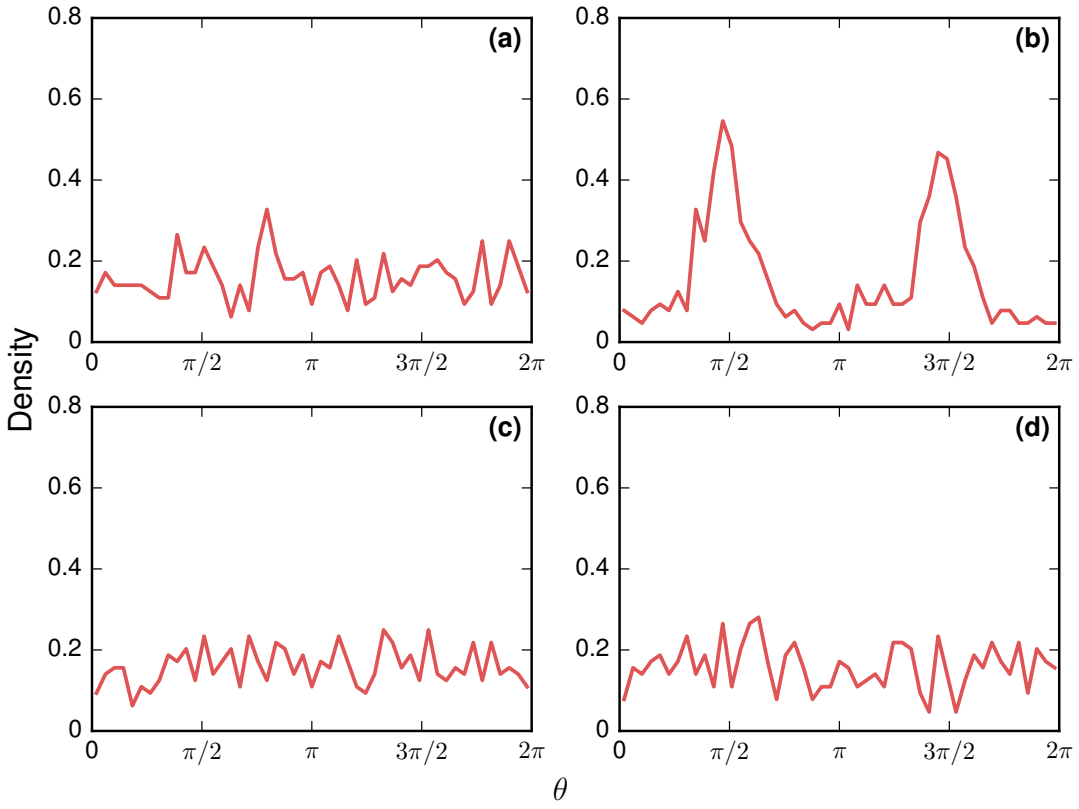

FIG. 4: Distribution of phases. Each curve represents a sampled density of the system presented in the main text, using $N = 500$, fourth-order Runge-Kutta integration with a step size of 0.01, 7500 transient steps, and uniformly random initial phases. (a) $K = 2$ and $J = 1$. (b) $K = 2$ and $J = 4$. (c) $K = 500$ and $J = 1$. (d) $K = 500$ and $J = 4$.

Appendix L: Persistence of incoherence

One common requirement for oscillator glasses is to demand that the phases of the oscillators be distributed uniformly. To measure this, we numerically compute the density of the phases θ_j, and plot the results in figure 4. Figure 4a shows the distribution at low K, below the volcano transition, and displays a uniform distribution. Figure 4b shows the distribution at low K, above the volcano transition, and exhibits substantial locking. Figure 4c shows the distribution at high K, below the volcano transition, and displays a uniform distribution. Figure 4d shows the distribution at high K, above the volcano transition, and displays a uniform distribution. This is consistent with the observation that high K (relative to N) may correspond to the onset of a glass, whereas low K definitely does not.

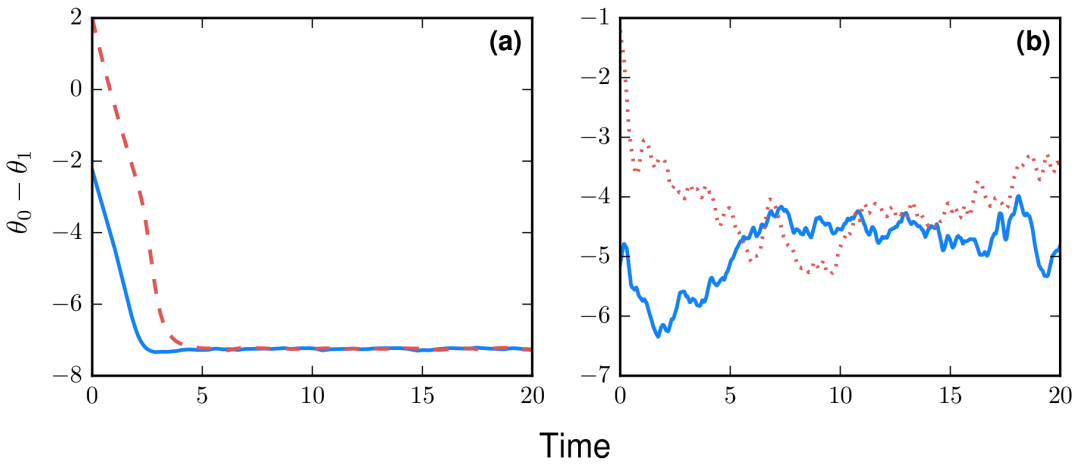

FIG. 5: Trajectory of phase differences. Each curve represents the difference between θ_0 and θ_1 of the system presented in the main text, using $N = 500$, fourth-order Runge-Kutta integration with a step size of 0.01 across 2000 steps, using uniformly random initial phases. The only difference between solid and dashed line in (a) (as well as in (b)) is the initial phases – the natural frequencies and coupling matrix remained identical. (a) $K = 2$ and $J = 4$. (b) $K = 500$ and $J = 4$.

Appendix M: Nonuniqueness of phase differences

Another common criterion for oscillator glasses is for there to be an abundance of attractors. One test of this is to test sensitivity to initial phases. That is, given a fixed pattern of natural frequencies and coupling strengths, and given locking oscillators θ_0 and θ_1, does the phase difference $\theta_0 - \theta_1$ depend on the choice of initial phases? Figure 5a suggests that different initial phases lead to the same asymptotic behavior in the low-K regime. However, figure 5b suggests a lack of any convergence in the high-K regime, consistent with the onset of glass.

[1] E. Ott and T. M. Antonsen, Chaos **18**, 037113 (2008) .